Jurnal Polimesin
Department of Mechanical Engineering
State Polytechnic of Lhokseumawe
http://e-jurnal.pnl.ac.id/polimesin
e-ISSN : 2549-1999 No. : 6 Month : December
p-ISSN : 1693-5462 Volume : 23 Year : 2025

Processing dates: received on 2025-10-2, reviewed on 2025-12-12, accepted on 2025-12-19 and online availability on 2025-12-31

Effect of nitrogen gas-assisted cooling on TIG weld distortion and mechanical properties of AA5083 aluminum alloy

Fuad Dwi Hanggara[1,*], Rama Dani Eka Putra[2], Tessa Zulenia Fitri[2], Handi Wilujeng Nugroho[3], Dhanang Suryo Prayogo[1]
[1]Mechanical Engineering, UIN Maulana Malik Ibrahim Malang, Malang 65144, Indonesia
[2]Industrial Engineering, Universitas Bengkulu, Bengkulu 38225, Indonesia
[3]Logistic Engineering, Universitas Sains dan Teknologi Indonesia, Pekanbaru 28294, Indonesia
*Corresponding author: fuaddh31@uin-malang.ac.id

Abstract

This study investigates the effect of nitrogen gas-assisted static cooling on weld distortion and mechanical properties of AA5083 aluminum alloy joined by Tungsten Inert Gas (TIG) welding. Although various cooling techniques have been reported to control heat input and distortion in aluminum welding, the combined influence of static nitrogen cooling and welding current on both distortion behavior and local mechanical properties of AA5083 remains insufficiently understood. Three welding current levels (100 A, 110 A, and 120 A) were applied while maintaining constant welding speed, arc voltage, and shielding gas flow. Mechanical properties, including tensile strength and Vickers hardness, were evaluated across the weld metal, Heat-Affected Zone (HAZ), and base metal. Thermal-induced distortion was analyzed using 3D profiling and validated through Analysis of Variance (ANOVA) statistical tests. The results indicate that a welding current of 100 A with static nitrogen cooling minimizes distortion and achieves the highest tensile strength (197.41 MPa). The highest yield strength was recorded at 120 A (160.31 MPa), while the maximum hardness values were observed in the weld metal at 110 A (135.83 VHN), HAZ at 120 A (117.63 VHN), and base metal at 100 A (124.1 VHN). Statistical analysis confirms that welding current significantly influences both distortion and mechanical outcomes ($p < 0.05$), while the cooling method shows a moderate effect. These findings demonstrate that nitrogen-assisted static cooling offers a practical approach to improving weld quality by balancing dimensional stability and mechanical performance in precision aluminum welding applications.

Keywords:
Distortortion, experimental, material, mechanical properties, welding.

1 Introduction

Aluminum and its alloys are widely employed nonferrous metals across key industrial sectors such as automotive, shipbuilding, petroleum, and aerospace [1], [2], [3]. With an annual global demand exceeding 24 million tons, aluminum serves as a crucial engineering material due to its excellent strength-to-weight ratio, corrosion resistance, and recyclability [4]. However, the relatively low mechanical strength of pure aluminum limits its use in structural applications, necessitating the development of aluminum alloys to enhance its performance characteristics [5], [6], [7]. Among the various aluminum alloy series, the 5xxx series (Al-Mg) has gained significant attention, particularly the AA5083 alloy, which contains approximately 4–5.5% magnesium [8], [9], [10]. This alloy is recognized for its high tensile strength, exceptional toughness at cryogenic temperatures, superior weld-ability, and outstanding corrosion resistance even in aggressive marine environments [11], [12]. As a result, AA5083 is extensively utilized in naval structures, pressure vessels, high-speed ships, and hull plating [13].

Welding is a fundamental process in the fabrication and joining of aluminum components [14], [15], [16]. However, welding thin aluminum plates (~3 mm thick), as often used in maritime applications, presents several technical challenges. These include residual stresses, thermal distortion, and changes in microstructure due to localized heat input during welding [17], [18]. Gas Tungsten Arc Welding (GTAW), or Tungsten Inert Gas (TIG) welding, is one of the most effective techniques for aluminum joining, providing high-quality and precision welds [19], [20]. Nevertheless, key welding parameters such as current intensity, electrode type, and shielding gas composition significantly influence the weld quality [21], [22], [23].

Argon is conventionally used as a shielding gas in TIG welding due to its inert nature and arc stability [24], [25]. However, conventional TIG welding still faces limitations in terms of heat input control, distortion management, and optimization of mechanical properties [26], [27], [28]. Therefore, strategies that can actively influence heat transfer and cooling behavior during or immediately after welding are of increasing interest.

Nitrogen gas is selected in this study primarily for its higher thermal conductivity and enhanced convective heat transfer capability, which can accelerate heat dissipation from the weld zone, reduce peak thermal gradients, and effectively control welding-induced distortion. In addition to its thermal role, modified cooling rates associated with nitrogen exposure may influence microstructural evolution in the weld metal and heat-affected zone, thereby affecting hardness and tensile behavior [29], [30], [31].

Despite these potential advantages, the combined effects of nitrogen-assisted static cooling and welding current on thermal distortion and local mechanical properties of AA5083 aluminum alloy have not been systematically investigated in previous studies. This lack of integrated thermal–mechanical analysis represents a clear research gap, particularly for thin aluminum plates used in marine and precision engineering applications.

Based on this gap, the present study systematically evaluates the influence of nitrogen gas-assisted static cooling during TIG welding of AA5083 aluminum alloy. The study focuses on clarifying how nitrogen-enhanced heat transfer interacts with welding current to affect tensile strength, hardness distribution, and thermal distortion. By linking thermal behavior, mechanical performance, and statistical analysis, this work provides a scientific basis for the application of nitrogen-assisted cooling as a practical strategy to improve weld quality and dimensional stability.

2 Research methodology

This study provides sufficient methodological detail to ensure reproducibility. Established methods are referenced, with only relevant modifications explained.

2.1 Materials specification

The material used in this study was AA5083-H116 aluminum alloy, selected for its favorable weld-ability, corrosion resistance, and mechanical strength. The nominal chemical composition of AA5083-H116 consists of 4.0–4.9 wt.% Mg, 0.4–1.0 wt.% Mn, up to 0.25 wt.% Cr, with minor amounts of Si (≤0.40 wt.%), Fe (≤0.40 wt.%), Cu (≤0.10 wt.%), Zn (≤0.25 wt.%), Ti (≤0.15 wt.%), and the balance aluminum. The typical mechanical properties include a yield strength of approximately 215 MPa, an ultimate tensile strength of 305–330 MPa, and an elongation of about 12–16%. The plates were prepared with dimensions of 150 mm × 100 mm × 6 mm. Prior to welding, the base metal surfaces were cleaned with acetone to remove surface contaminants and ensure consistent arc stability.

2.2 Welding process parameters

TIG welding was performed using a high-frequency AC TIG machine [32], [33]. Three levels of welding current were applied: 100 A, 110 A, and 120 A. Other process parameters were held constant: arc voltage at 18 V, travel speed at 5 mm·s^{-1}, and shielding gas flow rate at 15 L·min^{-1} using pure argon. A 2.4 mm thoriated tungsten electrode was used throughout all trials. For enhanced thermal control, a static nitrogen gas-assisted cooling setup was implemented [34]. Nitrogen was directed at the weld zone using a closed chamber system positioned underneath the specimen, allowing forced cooling immediately after the weld. Passed a water-cooling setup was also tested for comparison [35].

2.3 Experimental procedure

The experiment was designed using a full factorial design involving two independent factors: welding current and cooling method. The welding current factor consisted of three levels (100 A, 110 A, and 120 A), selected to examine the influence of increasing heat input on weld distortion and mechanical properties. The cooling method factor consisted of two levels: static nitrogen gas-assisted cooling and water cooling, chosen to compare gas-based convective cooling with a conventional liquid-based cooling approach. This resulted in a 3×2 full factorial experimental matrix, allowing the evaluation of both main effects and interaction effects between welding current and cooling method. For each factor combination, three replicate specimens were prepared to improve statistical reliability and reduce experimental variability. All welding operations were conducted in the flat (1G) position under identical environmental conditions [36], [37].

2.4 Mechanical testing

Tensile strength was measured using a Universal Testing Machine (UTM) with a capacity of 100 kN, in accordance with ASTM E8/E8M [38]. The specimens were machined perpendicular to the weld line, following sub-size standard gauge dimensions. The tensile test results showed an average yield strength of approximately 210 MPa, an ultimate tensile strength of 315 MPa, and an elongation of about 14%. Vickers hardness testing was performed according to ASTM E92 using a 100 g load and a dwell time of 15 seconds. Hardness measurements were conducted at three distinct zones, namely the weld metal, Heat-Affected Zone (HAZ), and base metal [39], [40], [41].

2.5 Distortion measurement

Distortion analysis was carried out using a digital height gauge to measure angular and longitudinal deviations before and after welding [42], [43]. Measurements were taken at three reference points along the plate edge to capture warping effects. Engineering strain ε relates the amount of deformation to the initial size of a sample in that direction. The formula is given by Eq. (1) [44], where ε is strain, ΔL is change in length and L_0 is initial length.

$$\varepsilon = \frac{\Delta L}{L_0} \tag{1}$$

Fig. 1 shows a schematic of the TIG welding process in which nitrogen (N_2) gas is directed toward the underside of the work-piece to provide static cooling, helping to control heat distribution and reduce welding-induced distortion.

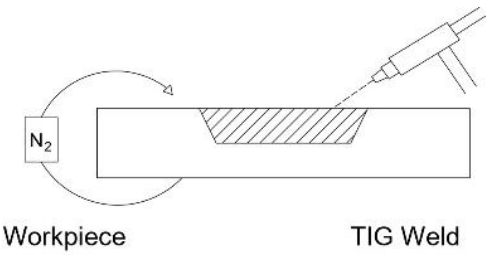

Fig. 1. Workpiece measurement.

2.6 Statistical analysis

All data were analyzed using two-way Analysis of Variance (ANOVA) to determine the significance of welding current and cooling method on mechanical properties and distortion [45], [46], [47], [48]. The assumptions of normality and homogeneity of variance were assessed through normal probability plots and Levene's test, respectively. Where significant main effects or interactions were found, Tukey's Honestly Significant Difference (HSD) test was conducted for pairwise comparison [49]. All statistical analyses were performed with a 95% confidence level (α = 0.05) [50], [51], [52]. These equations encompass the calculation of Degrees of Freedom (DOF), Sum of Squares (SS), Mean of Squares (MS), and F-values corresponding to each factor. The formulas are given by Eq. (2)-Eq. (12) [53], [54], [55], where SS_A is sum of squares between groups of factor A, SS_B is sum of squares between groups of factor B, SS_{AB} is sum of squares between groups of interaction AB, SS_E is sum of squares within groups (error), SS_T is total sum of squares, MS_A is mean squares between groups of factor A, MS_B is mean squares between groups of factor B, MS_{AB} is mean squares between groups of interaction AB, $\bar{Y}_{...}$ is overall average, $\bar{Y}_{i..}$ is average for level i on factor A, $\bar{Y}_{.j.}$ is average for level j on factor B, $\bar{Y}_{ij.}$ is combined average of the i-th level of A and the j-th level of B, n is number of samples, a is number of populations in factor A and b is number of populations in factor B.

1. Sum of Square (SS)

$$SS_A = bn\sum_{i=1}^{a}(Y_{i..} - \bar{Y}_{...})^2 \tag{2}$$

$$SS_B = an\sum_{j=1}^{b}\left(Y_{.j.} - \bar{Y}_{...}\right)^2 \tag{3}$$

$$SS_{AB} = n\sum_{i=1}^{a}\sum_{j=1}^{b}\left(\bar{Y}_{ij.} - \bar{Y}_{i..} - \bar{Y}_{.j.} + \bar{Y}_{...}\right)^2 \tag{4}$$

$$SS_T = \sum_{i=1}^{a}\sum_{j=1}^{b}\sum_{k=1}^{n}\left(Y_{ijk} - \bar{Y}_{...}\right)^2 \tag{5}$$

$$SS_E = \sum_{i=1}^{a}\sum_{j=1}^{b}\sum_{k=1}^{n}\left(Y_{ijk} - \bar{Y}_{ij.}\right)^2 \tag{6}$$

2. Mean Square (MS) and F-value (F)

$$MS_A = \frac{SS_A}{a-1} \tag{7}$$

$$MS_B = \frac{SS_B}{b-1} \tag{8}$$

$$MS_{AB} = \frac{SS_{AB}}{(a-1)(b-1)} \tag{9}$$

$$F_A = \frac{MS_A}{MS_E} \tag{10}$$

$$F_B = \frac{MS_B}{MS_E} \tag{11}$$

$$F_{AB} = \frac{MS_{AB}}{MS_E} \tag{12}$$

3 Results and discussion

It is appropriate to combine the results and discussion sections into a single section. Clear and concise results are required. The significance of the work's findings should be discussed in detail throughout the discussion section. Extensive citations and discussion of already published material should be avoided.

3.1 Weld distortion analysis

Distortion is a change in shape caused by heat, one of which is due to the welding process [56]. Due to this heating, grain elongation and rapid, non-uniform metal shrinkage occur, resulting in changes in shape and size (distortion) [57]. The data acquisition of current variation with cooling, as shown in Table 1.

Table 1. The Difference between current and type static cooling

Difference in test specimens	Type static cooling
Current 100 A	
Current 110 A	Water
Current 120 A	

3.2 Thermal-induced distortion analysis on aluminium 5083

Fig. 2 through Fig. 4 present the distortion behavior of AA5083 aluminum welds at varying welding currents (100 A, 110 A, and 120 A) under static water cooling. A 3D graphical analysis reveals that the welding current significantly affects the magnitude of angular distortion [58]. The distortion was found to be lowest at a welding current of 100 A, with maximum deviation occurring near the edges of the weld area. The peak distortion reached approximately 0.8 mm at the edge for the 100 A condition, while higher distortion levels were observed for 110 A and 120 A, with maxima exceeding 1.2 mm in certain regions. These results are attributed to the thermal gradients induced by arc heat input and subsequent non-uniform cooling [59]. The implementation of nitrogen gas-assisted cooling effectively moderated the heat input and provided a more uniform thermal dissipation, resulting in a reduction of residual stress and improved dimensional stability of the welded parts [60].

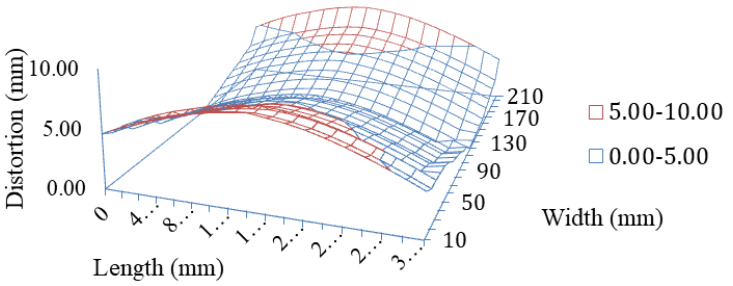

Fig. 2. 3D distortion chart for 100-Ampere current usage.

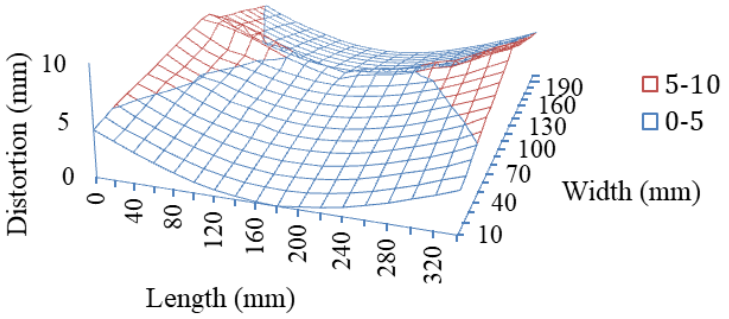

Fig. 3. 3D distortion chart for 110-Ampere current usage.

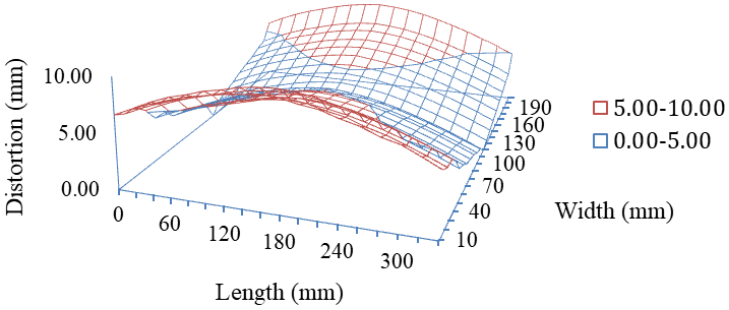

Fig. 4. 3D distortion chart for 120-Ampere current usage.

Based on the 3D graphical analysis presented in Fig. 2, the use of a welding current of 100 A resulted in a maximum distortion of 8 mm, observed at the coordinate position of 180 mm length and 240 mm width. The minimum distortion, measured at 0.12 mm, was located in a column with 360 mm length and 120 mm width. As shown in Fig. 3, when the welding current was increased to 110 A, the maximum distortion rose to 9.15 mm, located at 20 mm length and 110 mm width, while the minimum value was 0.10 mm, occurring at 160 mm length and 10 mm width. Furthermore, with a current of 120 A (Fig. 4), the highest distortion reached 10 mm at 180 mm length and 10 mm width, and the lowest distortion was 0.64 mm at the 340 mm length and 120 mm width.

From the three 3D distortion profiles, it can be concluded that welding current significantly affects the magnitude of distortion [58]. The lowest distortion occurred at 100 A, followed by 110 A, with the highest distortion observed at 120 A. This indicates that 100 A is the most optimal current setting to minimize distortion in the welding of AA5083 aluminum alloys. The distortion is primarily attributed to the residual stress generated during the welding process [61]. This stress arises from non-uniform thermal expansion between the weld metal and the base metal, particularly within the HAZ [62]. The thermal cycling during heating and cooling induces internal strains, which manifest as residual stresses that may cause bending, buckling, or localized warping, leading to measurable distortion in the material structure [63]. This finding supports the earlier work by Kadir *et al.*[64] and Verma & Pandey [65], which reported that increasing the welding current results in greater distortion. Therefore, controlling welding current is critical for preserving dimensional accuracy and structural stability, particularly in precision applications involving aluminum alloys [66], [67], [68].

3.3 Effect of longitudinal cooling on weld bead profile

Fig. 5 to Fig. 7 details the influence of cooling variation in the longitudinal direction on the material distortion. The longitudinal distortion results indicate that welding current has a significantly greater influence on distortion than the cooling area [69] [70]. Although static cooling reduced local thermal accumulation, its effect was secondary compared to the influence of current magnitude. This is supported by the ANOVA results (Table 2), where welding current showed a statistically significant effect ($p < 0.05$), while the cooling area did not.

These findings suggest that cooling strategies alone are insufficient to control distortion if excessive heat input is applied. Instead, distortion control in TIG welding of AA5083 requires a combined approach, where optimized welding current serves as the primary control parameter and cooling methods act as supplementary measures to enhance thermal dissipation [71] [72].

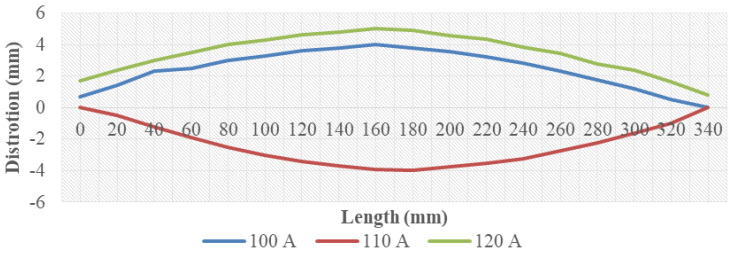

Fig. 5. Effect of longitudinal cooling on 10 mm bead distortion.

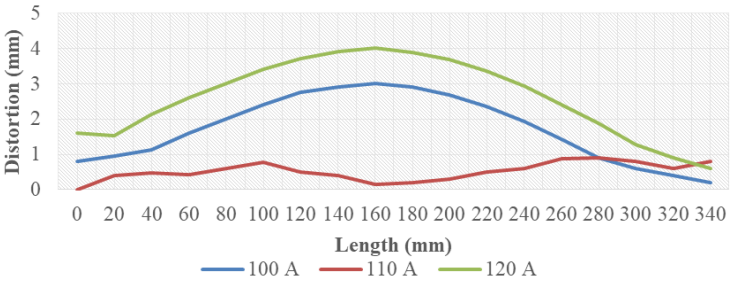

Fig. 6. Effect of longitudinal cooling on 120 mm bead distortion.

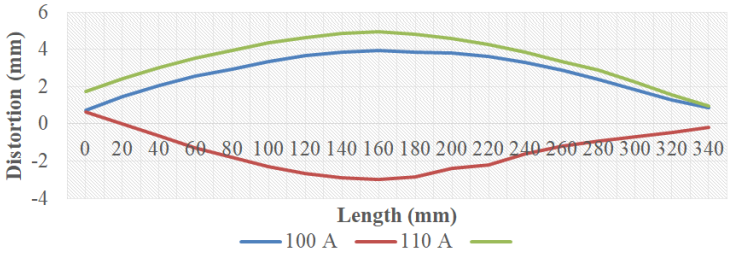

Fig.7. Effect of longitudinal cooling on 240 mm bead distortion.

The results of Table 2 ANOVA indicate that the welding current has a statistically significant effect on distortion values, with an F-value of 155.69 and a P-value of 0.000. This suggests that variations in current (100 A, 110 A, 120 A) lead to measurable differences in distortion. In contrast, the cooling area factor does not significantly affect distortion (F = 1.89; p = 0.155), indicating that within the tested range, changes in the cooling area do not statistically influence the distortion outcome.

Table 2. Two-way ANOVA: longitudinal cooling vs distortion

Analysis of variance					
Source	DF	Adj SS	Adj MS	F-value	P-value
Cooling area	2	7	3.334	1.89	0.155
Current	2	550.643	275.322	155.69	0
Error	157	277.647	1.768		
Lack of fit	4	89.928	22.482	18.32	0
Pure error	153	187.719	1.227		
Total	161	834.959			

These findings are consistent with the results reported by Selvamani *et al.* (2020), who observed that increasing welding current leads to greater distortion due to the increased heat input into the material. In welding processes, higher current typically results in a larger HAZ, which contributes to greater thermal deformation [73], [74], [75]. Similarly, Gautham *et al.* (2025) found that welding current is among the most influential parameters affecting weld quality, including distortion and tensile strength. Meanwhile, the insignificant effect of cooling the area in this study contrasts with the findings of Dekis *et al.* (2025), who reported that active cooling systems can significantly reduce distortion, especially in thin sheet metal welding. This discrepancy may stem from differences in the scale of cooling, cooling method, or material properties used in the respective studies [76] [77].

3.4 Tensile stress testing analysis

To evaluate the mechanical integrity of TIG-welded AA5083 aluminum, tensile and hardness testing were performed on different weldment regions under welding currents of 100 A, 110 A, and 120 A, as summarized in Table 3. The results indicate that the testing area within the weldment has a more pronounced influence on hardness variation than the welding current. The weld metal consistently exhibited higher hardness values compared to the HAZ and base metal, reflecting localized microstructural refinement associated with rapid solidification. Two-way ANOVA results (Table 4) confirm that the testing area significantly affects the mechanical response (p = 0.016), whereas variations in welding current within the investigated range do not produce a statistically significant effect. This finding suggests that microstructural heterogeneity inherent to welded joints governs mechanical performance more strongly than moderate changes in welding current. From a practical standpoint, these results imply that controlling weld zone characteristics is more critical than fine-tuning current levels when aiming to improve hardness distribution and overall weld performance in AA5083 TIG welds.

Table 3. Vickers Hardness (VHN) data at different welding currents

Testing area	Loop	100 A		110 A		120A	
		VHN	VHN rate	VHN	VHN rate	VHN	VHN rate
Base metal	1	124.9	124.1	123.2	122.2	124	122.8
	2	122		122.4		121.3	
	3	123		121		123.1	
HAZ	1	123.2	116.23	126.4	117.26	125.3	117.63
	2	125.3		123.3		123.9	
	3	100.2		102.1		103.7	
Weld metal	1	147.3	132.93	148.6	135.83	150.9	133.93
	2	114.2		115.4		113	
	3	137.3		143.5		137.9	

Table 4. Two way ANOVA tensile stress

Analysis of variance					
Source	DF	Adj SS	Adj MS	F-value	P-value
Cooling area	2	1.379	689.529	5.04	0.016
Current	2	4.27	2.085	0.02	0.985
Error	22	3011.77	136.899		
Lack of fit	4	13.83	3.456	0.02	0.999
Pure error	18	2997.94	166.552		
Total	26	4395			

A two-way ANOVA was conducted to evaluate the effects of two independent variables: testing area (base metal, heat affected zone, and weld metal) and current (100 A, 110 A, and 120 A) on the mechanical performance of welded aluminum specimens, with tensile strength or distortion values as the response variable. The ANOVA results indicate a statistically significant effect of the testing area on the response variable, with an F-value of 5.04 and a corresponding P-value of 0.016, which is less than the standard significance level of $\alpha = 0.05$. This suggests that the different regions within the weldment exhibit meaningful differences in mechanical behavior [78]. In contrast, the factor current yielded a P-value of 0.985 (F = 0.02), indicating that variations in the welding current within the range tested did not significantly influence the response variable [79].

The error term, with a relatively high adjusted Sum of Squares (SS = 3011.77) and Mean Square Error (MSE = 136.899), represents the variability not explained by the model. Notably, the lack of fit test produced a P-value of 0.999, suggesting that there is no significant deviation from model adequacy. This finding affirms that the selected model fits the data well, and the residual variation can be attributed to random or pure error rather than systematic inadequacies in the model structure [80]. Furthermore, the high value of pure error (SS = 2997.94) relative to the lack-of-fit supports the notion that variability is more likely due to replication differences among specimens rather than model misspecification.

In terms of hypothesis testing, the null hypothesis for the testing area (H_0: there is no difference in means among the testing zones) was rejected, indicating a significant effect of location within the welded material. Conversely, the null hypothesis for the current variable (H_0: there is no difference in means across current levels) was not rejected, implying that within the tested range, the magnitude of welding current did not significantly affect the mechanical response [81]. These results align with prior studies emphasizing the crucial role of metallurgical changes in different weld zones such as grain refinement and residual stress distribution in determining mechanical strength, while moderate changes in current may not exert substantial influence unless accompanied by more extreme variations in process parameters [21], [82]. Thus, the findings underscore the importance of microstructural zone characteristics over the applied current in influencing the outcome of welded joints [83].

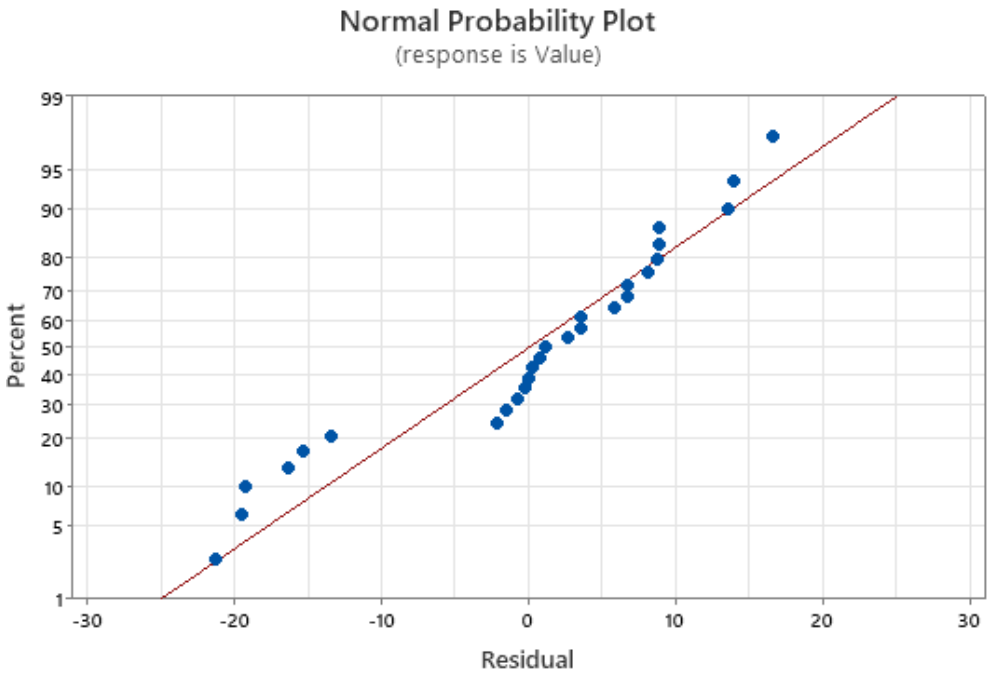

Fig. 8. Normal probability test.

The normal probability plot used to evaluate the normality assumption of the residuals shows that most points lie relatively close to the diagonal line, indicating that the residual distribution generally follows a normal distribution [84]. However, deviations are observed at the left and right tails of the plot, suggesting the presence of outliers or slight departures from normality. Nonetheless, in the context of ANOVA, the model is still considered valid, as ANOVA is known to be reasonably robust to minor violations of the normality assumption, particularly when the sample size is sufficiently large and the residual distribution does not exhibit severe skewness [67], [85], [86].

This condition indicates that the ANOVA model can be used to draw conclusions even in the presence of slight deviations in the residual data. To support this finding, additional analyses such as the Shapiro-Wilk or Anderson-Darling normality tests may be employed to numerically confirm the normality assumption [87]. Moreover, it is recommended to examine the potential presence of outliers to ensure that the interpretation of the ANOVA results remains accurate and unbiased. Therefore, the fundamental assumptions of ANOVA are generally satisfied, and the results of the analysis can still serve as a reliable basis for decision-making [88].

4 Conclusions

This study demonstrates that the use of static cooling in TIG welding with a current of 100 A is most effective in minimizing welding distortion while achieving the highest average tensile strength of 197.412 MPa. Based on the tensile test results presented in sub-section 3.4, the highest average yield strength was obtained at a welding current of 120 A, with a value of 160.315 MPa. The hardness results show a clear dependence on welding current and measurement zone. The weld metal exhibited the highest hardness at 110 A (135.83 VHN), which can be attributed to optimal heat input promoting finer microstructural features in the fusion zone. The maximum HAZ hardness was recorded at 120 A (117.63 VHN), likely due to increased thermal exposure causing microstructural transformation in this region. In contrast, the base metal hardness reached its highest value at 100 A (124.1 VHN), as lower heat input minimized thermal softening. These findings indicate that welding current plays a significant role in controlling heat input, which in turn affects both tensile properties and hardness distribution. To further optimize the welding process, it is recommended to explore a wider range of current settings, investigate alternative cooling methods beyond static cooling, and perform detailed microstructural analysis to better understand the effects of welding parameters on material behavior. Additionally, testing under different base metal conditions and dynamic loading scenarios such as fatigue and impact tests will provide a more comprehensive evaluation of weld quality and performance.

References

[1] M. Y. Khalid, R. Umer, and K. A. Khan, “Review of recent trends and developments in aluminium 7075 alloy and its metal matrix composites (MMCs) for aircraft applications,” *Results Eng.*, vol. 20, no. July, p. 101372, 2023, doi: 10.1016/j.rineng.2023.101372.

[2] N. Gharaibeh, M. AlAjlouni, and A. Al-Rousan, “Olive mill wastewater as cutting fluids: Effect on surface roughness of aluminum,” Jordan J. Mech. Ind. Eng., vol. 12, no. 3, pp. 161–166, 2019.

[3] N. Alshabatat and S. Al-qawabah, “Effect of 4 % wt . Cu Addition on the Mechanical Characteristics,” Jordan J. Mech. Ind. Eng., vol. 9, no. 4, pp. 297–301, 2015.

[4] S. Al-Alimi et al., “Recycling aluminium for sustainable development: A review of different processing technologies in green manufacturing,” Results Eng., vol. 23, no. November 2023, p. 102566, 2024, doi: 10.1016/j.rineng.2024.102566.

[5] Y. M. Altharan, S. Shamsudin, S. Al-Alimi, Y. Saif, and W. Zhou, “A review on solid-state recycling of aluminum machining chips and their morphology effect on recycled part quality,” Heliyon, vol. 10, no. 14, p. e34433, 2024, doi: 10.1016/j.heliyon.2024.e34433.

[6] X. You et al., “A review of research on aluminum alloy materials in structural engineering,” Dev. Built Environ., vol. 17, no. January, p. 100319, 2024, doi: 10.1016/j.dibe.2023.100319.

[7] Y. Liu, L. He, and S. Yuan, “Wear Properties of Aluminum Alloy 211z.1 Drilling Tool,” Jordan J. Mech. Ind. Eng., vol. 15, no. 1, pp. 59–63, 2021.

[8] M. Sarıkaya, D. Başcıl Önler, S. Dağlı, S. Hartomacıoğlu, M. Günay, and G. M. Królczyk, “A review on aluminum alloys produced by wire arc additive manufacturing (WAAM): Applications, benefits, challenges and future trends,” J. Mater. Res. Technol., vol. 33, no. September, pp. 5643–5670, 2024, doi: 10.1016/j.jmrt.2024.10.212.

[9] H. Zhu and J. Li, “Advancements in corrosion protection for aerospace aluminum alloys through surface treatment,” Int. J. Electrochem. Sci., vol. 19, no. 2, p. 100487, 2024, doi: 10.1016/j.ijoes.2024.100487.

[10] Tiwan, M. N. Ilman, and Kusmono, "Microstructure and mechanical properties of friction stir spot welded AA5052-H112 aluminum alloy," Heliyon, vol. 7, no. 2, p. e06009, 2021, doi: 10.1016/j.heliyon.2021.e06009.
[11] M. Vakili, P. Koutník, J. Kohout, and Z. Gholami, "Analysis, Assessment, and Mitigation of Stress Corrosion Cracking in Austenitic Stainless Steels in the Oil and Gas Sector: A Review," Surfaces, vol. 7, no. 3, pp. 589–642, 2024, doi: 10.3390/surfaces7030040.
[12] Q. Xiao, Y. Xie, F. Hu, and C. Hu, "Current Status and Trends of Low-Temperature Steel Used in Polar Regions," Materials (Basel)., vol. 17, no. 13, 2024, doi: 10.3390/ma17133117.
[13] V. T. Doan, B. Liu, Y. Garbatov, W. Wu, and C. Guedes Soares, "Strength assessment of aluminium and steel stiffened panels with openings on longitudinal girders," Ocean Eng., vol. 200, no. January, p. 107047, 2020, doi: 10.1016/j.oceaneng.2020.107047.
[14] H. Ghari, A. Taherizadeh, B. Sadeghian, B. Sadeghi, and P. Cavaliere, Metallurgical characteristics of aluminum-steel joints manufactured by rotary friction welding: A review and statistical analysis, vol. 30, no. January. Elsevier B.V., 2024. doi: 10.1016/j.jmrt.2024.03.089.
[15] Y. Ning, Z. Qiu, B. Wu, Z. Pan, and H. Li, "Hardfacing of metals : A review of consumables , properties and strengthening processes," J. Mater. Res. Technol., vol. 36, no. April, pp. 6330–6349, 2025, doi: 10.1016/j.jmrt.2025.04.221.
[16] B. B. Sherpa and R. Rani, "Advancements in explosive welding process for bimetallic material joining: A review," J. Alloy. Metall. Syst., vol. 6, no. May, p. 100078, 2024, doi: 10.1016/j.jalmes.2024.100078.
[17] D. Xie et al., "A Review on Distortion and Residual Stress in Additive Manufacturing," Chinese J. Mech. Eng. Addit. Manuf. Front., vol. 1, no. 3, p. 100039, 2022, doi: 10.1016/j.cjmeam.2022.100039.
[18] S. Liu et al., "Optimization of welding parameters on welding distortion and stress in S690 high-strength steel thin-plate structures," J. Mater. Res. Technol., vol. 25, pp. 382–397, 2023, doi: 10.1016/j.jmrt.2023.05.169.
[19] V. M. Gautham, A. Sumesh, E. V. Jithin, K. Rameshkumar, and D. T. Thekkuden, "Evaluation of Time-Domain Acoustic Signature in TIG Welding of 5083 Aluminum Alloy: A Methodological Comparison of Feature Reduction Approaches," Results Eng., vol. 26, no. April, p. 105062, 2025, doi: 10.1016/j.rineng.2025.105062.
[20] R. Casanueva, C. Brañas, F. J. Diaz, F. J. Azcondo, D. Ferreño, and J. Setien, "Characterization of an energy efficient pulsed current TIG welding process on AISI 316 and 304 stainless steels," Heliyon, vol. 9, no. 9, pp. 1–13, 2023, doi: 10.1016/j.heliyon.2023.e19819.
[21] M. K. Dezfuli, A. H. Moghadam, M. G. Hasab, and R. Ashiri, "Effect of pulsed current frequency on alloy chemistry , microstructure , and mechanical responses of Hastelloy B-2 superalloy in gas tungsten arc welding process," J. Mater. Res. Technol., vol. 36, no. April, pp. 6950–6968, 2025, doi: 10.1016/j.jmrt.2025.04.293.
[22] R. P. Verma, K. N. Pandey, K. András, R. Khargotra, and T. Singh, "Difficulties and redressal in joining of aluminium alloys by GMA and GTA welding: a review," J. Mater. Res. Technol., vol. 23, pp. 2576–2586, 2023, doi: 10.1016/j.jmrt.2023.01.183.
[23] P. Muangjunburee, H. Z. Oo, S. Z. A. Rahim, and B. Srikarun, "Abrasive wear performance of repair welds on R260 rail using different welding electrodes," Results Eng., vol. 26, no. December 2024, p. 104680, 2025, doi: 10.1016/j.rineng.2025.104680.
[24] P. Murali and R. Gopi, "Experimental investigation of tungsten inert gas welding (TIG) using Ar/Ar-CO2 shielding gas on alloy steels," Mater. Today Proc., vol. 39, no. xxxx, pp. 812–817, 2020, doi: 10.1016/j.matpr.2020.09.776.
[25] E. A. Chiniforoush, T. Gholizadeh, M. R. Jandaghi, J. Moverare, and C. H. Gür, "Impact of active to inert shielding gas transition on the corrosion behavior of wire arc additively manufactured duplex stainless steel," Mater. Des., vol. 253, no. April, p. 113907, 2025, doi: 10.1016/j.matdes.2025.113907.
[26] K. Szwajka, J. Zielińska-Szwajka, and T. Trzepieciński, "The Influence of the Shielding-Gas Flow Rate on the Mechanical Properties of TIG-Welded Butt Joints of Commercially Pure Grade 1 Titanium," Materials (Basel)., vol. 17, no. 5, 2024, doi: 10.3390/ma17051217.
[27] P. N. Bellamkonda, M. Dwivedy, and R. Addanki, "Cold metal transfer technology - A review of recent research developments," Results Eng., vol. 23, no. April, p. 102423, 2024, doi: 10.1016/j.rineng.2024.102423.
[28] N. A. Siddiqui, M. Muzamil, T. Jamil, and G. Hussain, "Heat sources in wire arc additive manufacturing and their impact on macro-microstructural characteristics and mechanical properties – An overview," Smart Mater. Manuf., vol. 3, no. May 2024, p. 100059, 2025, doi: 10.1016/j.smmf.2024.100059.
[29] N. Tapoglou, J. Clulow, and D. Curtis, "Increased shielding of a Direct Energy Deposition process to enable Deposition of reactive materials; an investigation into Deposition of 15-5 PH Stainless Steel, Inconel 718 and Ti-6Al-4V," CIRP J. Manuf. Sci. Technol., vol. 36, no. xxxx, pp. 227–235, 2022, doi: 10.1016/j.cirpj.2020.11.013.
[30] J. Ning, S. J. Na, C. hong Wang, and L. J. Zhang, "A comparison of laser-metal inert gas hybrid welding and metal inert gas welding of high-nitrogen austenitic stainless steel," J. Mater. Res. Technol., vol. 13, pp. 1841–1854, 2021, doi: 10.1016/j.jmrt.2021.05.113.
[31] Q. Shao et al., "Study of repair welding on microstructure, mechanical properties and corrosion resistance of dissimilar welded joints of SUS304 and Q345B steel," J. Mater. Res. Technol., vol. 23, pp. 4173–4189, 2023, doi: 10.1016/j.jmrt.2023.02.061.
[32] H. He et al., "Optimization of Joining Parameters in Pulsed Tungsten Inert Gas Weld Brazing of Aluminum and Stainless Steel Based on Response Surface Methodology," Coatings, vol. 14, no. 10, 2024, doi: 10.3390/coatings14101262.
[33] Y. Hu, W. Pei, H. Ji, R. Yu, and S. Liu, "Tungsten Inert Gas Welding of 6061-T6 Aluminum Alloy Frame: Finite Element Simulation and Experiment," Materials (Basel)., vol. 17, no. 5, 2024, doi: 10.3390/ma17051039.
[34] Y. G. Lv, Y. T. Wang, T. Meng, Q. W. Wang, and W. X. Chu, "Review on thermal management technologies for electronics in spacecraft environment," Energy Storage Sav., vol. 3, no. 3, pp. 153–189, 2024, doi: 10.1016/j.enss.2024.03.001.
[35] S. M. Shalaby, M. K. Elfakharany, B. M. Moharram, and H. F. Abosheiasha, "Experimental study on the performance of PV with water cooling," Energy Reports, vol. 8, pp. 957–961, 2022, doi: 10.1016/j.egyr.2021.11.155.
[36] L. Atia and M. Bamberger, "Development of coated electrodes for welding of Super Duplex steel," Heliyon, vol. 6, no. 1, p. e02907, 2020, doi: 10.1016/j.heliyon.2019.e02907.
[37] H. Alipooramirabad, A. Paradowska, M. Reid, and R. Ghomashchi, "Post weld heat treatment of bisalloy 80 steel: Mechanics and industry safety code compatibility," Int. J. Press. Vessel. Pip., vol. 214, no. December 2024, p. 105434, 2025, doi: 10.1016/j.ijpvp.2025.105434.
[38] S. Y. Hiew et al., "A unified tensile constitutive model for mono/hybrid fibre-reinforced ultra-high-performance concrete (UHPC)," Cem. Concr. Compos., vol. 150, no. November 2023, p. 105553, 2024, doi: 10.1016/j.cemconcomp.2024.105553.

[39] L. Zhou, T. Lin, P. Xu, Z. Jiang, and Y. Liang, "Grain gradient in the heat-affected zone acquires an advancement in the ductility of flash-butt welded IN718 alloy," J. Mater. Res. Technol., vol. 33, no. August, pp. 4938–4951, 2024, doi: 10.1016/j.jmrt.2024.10.100.
[40] K. Z. Ghumman, S. Ali, E. U. Din, A. Mubashar, N. B. Khan, and S. W. Ahmed, "Experimental investigation of effect of welding parameters on surface roughness, micro-hardness and tensile strength of AISI 316L stainless steel welded joints using 308L filler material by TIG welding," J. Mater. Res. Technol., vol. 21, pp. 220–236, 2022, doi: 10.1016/j.jmrt.2022.09.016.
[41] S. Shojai, F. Schönamsgruber, M. Köhler, and E. Ghafoori, "Impact of accelerated corrosion on weld geometry, hardness and residual stresses of offshore steel joints over time," Mater. Des., vol. 251, no. July 2024, 2025, doi: 10.1016/j.matdes.2024.113578.
[42] Y. Al-zain, "Glass-Reinforced Aluminum Matrix Composite : Synthesizes , Neural Networks," vol. 1, no. 3, pp. 509–519, 2024.
[43] B. Zhao, "Multi-Layer and Multi-Channel Welding Trajectory Control Method of Welding Robot," Jordan J. Mech. Ind. Eng., vol. 16, no. 1, pp. 153–162, 2022.
[44] S. Kar, J. L. Cuddigan, and M. L. Greenfield, "Simulating Stress–Strain Behavior by Using Individual Chains: Uniaxial Deformation of Amorphous Cis- and Trans-1,4-Polybutadiene," Polymers (Basel)., vol. 15, no. 6, pp. 1–22, 2023, doi: 10.3390/polym15061441.
[45] V. Kumar, "Modeling of weld bead geometry and shape relationships in submerged arc welding using developed fluxes," Jordan J. Mech. Ind. Eng., vol. 5, no. 5, pp. 461–470, 2011.
[46] M. Waqas, A. Israr, M. E. Qureshi, M. Muzamil, and A. Majeed, "Experimental and statistical investigation of laser welding with different joint gap widths for HSLA steel," Smart Mater. Manuf., vol. 2, no. April, pp. 1–19, 2024, doi: 10.1016/j.smmf.2024.100057.
[47] R. Schur et al., "Mechanical anisotropy and its evolution with powder reuse in Electron Beam Melting AM of Ti6Al4V," Mater. Des., vol. 200, p. 109450, 2021, doi: 10.1016/j.matdes.2021.109450.
[48] S. H. Aghdeab, L. A. Mohammed, and A. M. Ubaid, "Optimization of CNC turning for aluminum alloy using simulated annealing method," Jordan J. Mech. Ind. Eng., vol. 9, no. 1, pp. 39–44, 2015.
[49] J. A. Fryer, A. Dupas de Matos, J. Hort, and E. Tomasino, "Consumer responses to smoke-impacted pinot noir wine and the influence of label concepts on perception," Food Res. Int., vol. 203, no. January, p. 115881, 2025, doi: 10.1016/j.foodres.2025.115881.
[50] S. Oliveira, I. Sousa, and A. Raymundo, "Printability evaluation of Chlorella vulgaris snacks," Algal Res., vol. 68, no. November 2021, p. 102879, 2022, doi: 10.1016/j.algal.2022.102879.
[51] [Z. Chen et al., "Oil and gas platforms degrade benthic invertebrate diversity and food web structure," Sci. Total Environ., vol. 929, no. April, p. 172536, 2024, doi: 10.1016/j.scitotenv.2024.172536.
[52] J. Cuartero et al., "Earthworm and enchytraeid indicator taxa of different land-use types identified using soil DNA metabarcoding," Appl. Soil Ecol., vol. 206, no. January, 2025, doi: 10.1016/j.apsoil.2025.105891.
[53] T. Gadrich and Y. N. Marmor, "Two-way ORDANOVA: Analyzing ordinal variation in a cross-balanced design," J. Stat. Plan. Inference, vol. 215, pp. 330–343, 2021, doi: 10.1016/j.jspi.2021.04.005.
[54] S. Afzal, M. Rauf, S. Ashraf, S. Bin Md Ayob, and Z. Ahmad Arfeen, "CART-ANOVA-Based Transfer Learning Approach for Seven Distinct Tumor Classification Schemes with Generalization Capability," Diagnostics, vol. 15, no. 3, 2025, doi: 10.3390/diagnostics15030378.
[55] J. C. W. Rayner and G. C. Livingston, "Testing for Level–Degree Interaction Effects in Two-Factor Fixed-Effects ANOVA When the Levels of Only One Factor Are Ordered," Stats, vol. 7, no. 2, pp. 481–491, 2024, doi: 10.3390/stats7020029.
[56] H. D. Seo and J. M. Lee, "A new welding distortion analysis method considering inherent deformation-based tendon force estimation," Int. J. Nav. Archit. Ocean Eng., vol. 17, no. July 2024, p. 100640, 2025, doi: 10.1016/j.ijnaoe.2024.100640.
[57] R. M. German, "Sintered tungsten heavy alloys: Review of microstructure, strength, densification, and distortion," Int. J. Refract. Met. Hard Mater., vol. 108, no. July, p. 105940, 2022, doi: 10.1016/j.ijrmhm.2022.105940.
[58] J. Yang, P. Cao, J. Yao, J. Wang, Q. Mao, and Y. Yang, "Optimization of Plasma Welding Sequence and Performance Verification for a Fork Shaft: A Comparison of Same-Direction and Reverse-Direction Welding," Materials (Basel)., vol. 18, no. 2, 2025, doi: 10.3390/ma18020288.
[59] B. Yelamasetti, S. P. Sushma, Z. Mohammed, H. Altammar, M. F. Khan, and S. Q. Moinuddin, "Synergistic Effects of Thermal Cycles and Residual Stress on Microstructural Evolution and Mechanical Properties in Monel 400 and AISI 316L Weld Joints," 2025.
[60] S. Chen, H. Gao, Y. Zhang, Q. Wu, Z. Gao, and X. Zhou, "Review on residual stresses in metal additive manufacturing: formation mechanisms, parameter dependencies, prediction and control approaches," J. Mater. Res. Technol., vol. 17, pp. 2950–2974, 2022, doi: 10.1016/j.jmrt.2022.02.054.
[61] S. Das Banik, S. Kumar, P. K. Singh, S. Bhattacharya, and M. M. Mahapatra, "Prediction of distortions and residual stresses in narrow gap weld joints prepared by hot wire GTAW and its validation with experiments," Int. J. Press. Vessel. Pip., vol. 193, no. June, p. 104477, 2021, doi: 10.1016/j.ijpvp.2021.104477.
[62] J. S. Roh and M. H. Kim, "Mitigation of the residual stress and deformation in seam pipe with girth welding and cutting," Int. J. Nav. Archit. Ocean Eng., vol. 17, no. January, p. 100657, 2025, doi: 10.1016/j.ijnaoe.2025.100657.
[63] H. Chae et al., "Unravelling thermal history during additive manufacturing of martensitic stainless steel," J. Alloys Compd., vol. 857, 2021, doi: 10.1016/j.jallcom.2020.157555.
[64] M. H. A. Kadir, M. Asmelash, and A. Azhari, "Investigation on welding distortion in stainless steel sheet using gas tungsten arc welding process," Mater. Today Proc., vol. 46, no. xxxx, pp. 1674–1679, 2020, doi: 10.1016/j.matpr.2020.07.264.
[65] R. P. Verma and K. N. Pandey, "Multi-response optimization of process parameters of GMA welding of dissimilar AA 6061-T6 and AA 5083-O aluminium alloy for optimal mechanical properties," Mater. Today Proc., vol. 46, no. xxxx, pp. 10204–10210, 2021, doi: 10.1016/j.matpr.2020.11.375.
[66] A. Sahoo, S. Tripathy, and D. K. Tripathy, "Parametric Optimization of Pulse TIG Welding Process during Joining of Dissimilar Tensile Steels Used in Automotive Industries," Jordan J. Mech. Ind. Eng., vol. 16, no. 5, pp. 663–676, 2022.
[67] S. Dwivedi and S. Sharma, "Optimization of resistance spot welding process parameters on shear tensile strength of SAE 1010 steel sheets joint using Box-Behnken design," Jordan J. Mech. Ind. Eng., vol. 10, no. 2, pp. 115–122, 2016.
[68] B. S. BAYRAM, M. O. KABAKÇI, and İ. KORKUT, "Investigation of the Milling Methods Effects on Machining Performance of AA 7075-T6 Aluminum Alloy and Process Parameters Optimization," Jordan J. Mech. Ind. Eng., vol. 19, no. 1, pp. 91–104, 2025, doi: 10.59038/jjmie/190107.
[69] S. Suman and P. Biswas, "Finite element analysis of in-process thermal mitigation of welding induced residual stresses

in 9Cr-1Mo-V steel butt joint considering phase transformation," J. Manuf. Process., vol. 70, no. September, pp. 361–375, 2021, doi: 10.1016/j.jmapro.2021.08.027.
[70] I. Okta, S. M. Sultan, A. Fudholi, M. Mohammad, and C. P. Tso, "Case Studies in Thermal Engineering A new cooling method for photovoltaic module using U-shape aluminum fins and circular copper tubes : An indoor experiment and economic study," Case Stud. Therm. Eng., vol. 72, no. March, p. 106396, 2025, doi: 10.1016/j.csite.2025.106396.
[71] S. T. Selvamani, S. Velmurugan, V. Balasubramanian, and K. Palanikumar, "Effects of heat distribution during cold metal transfer arc welding on galvanized steel using volumetric heat source model," J. Mater. Res. Technol., vol. 9, no. 5, pp. 10097–10109, 2020, doi: 10.1016/j.jmrt.2020.07.004.
[72] R. Dhairiyasamy and D. Gabiriel, "Enhancing Corrosion Resistance and Mechanical Strength in Dissimilar Steel Welding Through Controlled Waveform," vol. 19, no. 1, pp. 179–192, 2025.
[73] Z. Yao, M. Omiya, N. Ma, P. Geng, and Q. Wang, "Local shear fracture properties in heat-affected zone of resistance spot-welded advanced high-strength steel," J. Mater. Res. Technol., vol. 32, no. August, pp. 2200–2213, 2024, doi: 10.1016/j.jmrt.2024.08.035.
[74] S. Baek et al., "Al heat affected zone-less resistance element welded lap joints of Al alloy and 1 GPa class steel: Transition of microstructure and fracture with heat transfer," J. Mater. Res. Technol., vol. 28, no. December 2023, pp. 3541–3565, 2024, doi: 10.1016/j.jmrt.2023.12.210.
[75] M. Dekis, M. Tawfik, M. Egiza, and M. Dewidar, "Challenges and developments in wire arc additive manufacturing of steel: A review," Results Eng., vol. 26, no. May 2024, p. 104657, 2025, doi: 10.1016/j.rineng.2025.104657.
[76] A. U. Yakubu et al., "A comprehensive review of primary cooling techniques and thermal management strategies for polymer electrolyte membrane fuel cells PEMFC," Heliyon, vol. 10, no. 19, p. e38556, 2024, doi: 10.1016/j.heliyon.2024.e38556.
[77] M. Zarei, M. G. Shabestari, S. G. Shabestari, and H. Abedi, "Microstructural heterogeneity and anisotropic mechanical propertiers of titanium alloys manufactured by wire arc additive manufacturing : A review," J. Mater. Res. Technol., vol. 36, no. May, pp. 8381–8409, 2025, doi: 10.1016/j.jmrt.2025.05.106.
[78] M. H. Amini-Chelak, R. Miresmaeili, M. Askari-Paykani, H. Aliyari, and H. R. Shahverdi, "Resistance spot weldability of Fe66Cr16.5Ni14.1Si3.4 advanced high strength steel using D-optimal design of experiment method," J. Mater. Res. Technol., vol. 25, pp. 5615–5632, 2023, doi: 10.1016/j.jmrt.2023.06.262.
[79] S. M. Rahman, J. Carlson, S. P. Gudergan, M. Wetzels, and D. Grewal, "Perceived Omnichannel Customer Experience (OCX): Concept, measurement, and impact," J. Retail., vol. 98, no. 4, pp. 611–632, 2022, doi: 10.1016/j.jretai.2022.03.003.
[80] C. P. Tamil Selvan, I. Dinaharan, R. Palanivel, and K. Kalaiselvan, "Predicting the tensile strength and deducing the role of processing conditions of hot wire gas tungsten arc welded pure nickel tubes using an empirical relationship," Int. J. Press. Vessel. Pip., vol. 188, no. October, p. 104220, 2020, doi: 10.1016/j.ijpvp.2020.104220.
[81] E. Ahmed et al., "Lightweight aluminum joint design: Enhancement of mechanical properties through novel inter-layer and powder additives in friction stir welding," Int. J. Light. Mater. Manuf., vol. 8, no. 3, pp. 341–354, 2025, doi: 10.1016/j.ijlmm.2025.02.001.
[82] Z. Tao et al., "Effect of heat input on microstructural evolution and impact toughness in dissimilar weld metals between medium Mn and V-microalloyed steel," Alexandria Eng. J., vol. 114, no. May 2024, pp. 95–111, 2025, doi: 10.1016/j.aej.2024.11.082.
[83] N. Hernandez, F. Carrillo-Perez, F. M. Ortuño, I. Rojas, and O. Valenzuela, "Understanding the Impact of Deep Learning Model Parameters on Breast Cancer Histopathological Classification Using ANOVA," Cancers (Basel)., vol. 17, no. 9, pp. 1–24, 2025, doi: 10.3390/cancers17091425.
[84] S. P. Dwivedi and R. Sahu, "Effects of SiC particles parameters on the corrosion protection of aluminum-based metal matrix composites using response surface methodology," Jordan J. Mech. Ind. Eng., vol. 12, no. 4, pp. 313–321, 2018.
[85] S. A. Rizvi and S. P. Tewari, "Optimization of welding parameters by using Taguchi method and study of fracture mode characterization of SS304H welded by GMA welding," Jordan J. Mech. Ind. Eng., vol. 12, no. 1, pp. 17–22, 2018.
[86] V. Manchaiah, G. Andersson, E. W. Beukes, M. A. Fagelson, D. W. Swanepoel, and D. Maidment, "Changes in Perceived Tinnitus Sound Qualities Following Internet-Based Cognitive Behavioral Therapy for Tinnitus," Clin. Pract., vol. 15, no. 4, pp. 1–11, 2025, doi: 10.3390/clinpract15040069.
[87] J. Arnastauskaitė, T. Ruzgas, and M. Bražėnas, "An exhaustive power comparison of normality tests," Mathematics, vol. 9, no. 7, pp. 1–20, 2021, doi: 10.3390/math9070788.
[88] L. Platz and M. Zauner, "Financial Literacy Games—Increasing Utility Value by Instructional Design in Upper Secondary Education," Educ. Sci., vol. 15, no. 2, pp. 1–16, 2025, doi: 10.3390/educsci15020227.